Normal Force Calculations for Rocket-like Configurations

E. D. V. Bigarella
Instituto Tecnológico de Aeronáutica
S.J. Campos, SP, Brazil
enda.bigarella@ig.com.br

J. L. F. Azevedo
O. A. F. Mello
Instituto de Aeronáutica e Espaço
CTA/IAE/ASE-N
S.J. Campos, SP, Brazil
azevedo@iae.cta.br
oamello@directnet.com.br

Transonic and supersonic flow simulations over typical launch vehicle configurations are presented. A 3-D finite difference numerical code, written for general, curvilinear, body-conforming coordinate systems, is used. The code solves the thin-layer approximation for the laminar Navier-Stokes equations. Simulations are performed for a launcher and a sounding rocket configurations, currently under development at Instituto de Aeronáutica e Espaço. Calculations consider cases at angle of attack and at various freestream Mach numbers. Normal force coefficients are obtained such that the loads required for the design phase can be determined. Computational results are compared to available experimental data. In general, good results within engineering error margins are obtained.
***Keywords**: CFD, viscous flows, aerospace configurations, design application*

Introduction

Launch vehicles are typically designed to fly at very low angles of attack. Nevertheless, even at such low angles of attack, the lateral loads that arise in these vehicles are quite strong and they must be accurately determined. Therefore, during the design process, one is required to determine the aerodynamics of these vehicles at angle of attack because this will provide the loads required for the structural design of the vehicle as well as the flight dynamics stability characteristics necessary for the control system design. Earlier work (Zdravistch and Azevedo, 1990; Azevedo, Zdravistch and Silva, 1991) has presented axisymmetric viscous simulations for flows over the first Brazilian Satellite Launch Vehicle (VLS) with very good representation of the flow physics. Moreover, 3-D inviscid computations over the VLS, at low angles of attack, were also performed (Azevedo *et al*, 1996) with good agreement with experimental data.

This earlier work, however, considered fairly simple 3-D geometries and, typically, mesh refinement was less than adequate due to computational resource limitations. This discussion emphasizes that the problem of simulating transonic and supersonic flows over complex vehicles is not a new requirement at Instituto de Aeronáutica e Espaço (IAE). However, more recent development of the computational tools available in the computational fluid dynamics (CFD) group (Basso, Antunes and Azevedo, 2000a), together with additional computational resources available in the country, have made possible the analysis of almost realistic configurations. In this context, Basso, Antunes and Azevedo (2000b) presented results for the complete, 1st-stage flight, VLS configuration. The comparisons included in that work considered solely flight conditions at zero angle of attack. The present work, despite the fact that it does not include the VLS lateral boosters in the analyzed configurations, is aimed at studying the behavior of running normal force coefficients and normal force coefficient slopes as a function of Mach number. These analyses are closer to the primary aerodynamic data that the designer needs in order to assess structural loads and control system effectiveness. Moreover, they require the consideration of flight conditions at angle of attack.

Hence, the computational code is used to simulate the 3-D flows about two vehicles now under development at IAE, namely the VLS and the Sonda III-A sounding rocket, at different angles of attack and for various freestream Mach numbers. The VLS is a four-stage satellite launcher built with four booster attached to a main body. In the present work, computations were performed considering only the vehicle central body. The solver used is a 3-D finite-difference code written for general, body-conforming, curvilinear coordinate systems and solves the thin-layer approximation of the compressible laminar Navier-Stokes equations.

It should be remarked that the complete representation of the flowfields of interest should consider a turbulent viscous formulation. Actual flight Reynolds numbers for the vehicles are very large, of the order of 10^7, and some relevant phenomena defining the flow topology require a viscous turbulent formulation. Nevertheless, this paper includes only Navier-Stokes results without turbulence closure, since it is an account of the evolutionary process towards the complete flow simulation capability desired. These results are necessary in order to address the level of accuracy that can be attained with the computational tool under development. Furthermore, as the discussion in the paper will show, the results that can be obtained with the current formulation are already useful from an engineering standpoint and, in the Sonda III-A case, they have actually been used for aerodynamic design.

Nomenclature

a = Sound speed
CFL = Courant-Friedrichs-Levy number
CN = Normal force coefficient
CN_α = Normal force coefficient slope
Cp = Pressure coefficient
d = Artificial dissipation term
d = Dimensional vehicle diameter
e = Total energy per unit volume
$\overline{E},\overline{F},\overline{G}$ = Dimensionless inviscid flux vectors in general curvilinear coordinates
$\overline{E_v},\overline{F_v},\overline{G_v}$ = Dimensionless viscous flux vectors in general curvilinear coordinates
J = Jacobian of the coordinate transformation
M = Mach number
$\overline{Q}$ = Dimensionless array of conserved properties
Re = Reynolds number
RHS = Right-hand side operator
u, v, w = Velocity components in Cartesian coordinates

Greek Characters

α = Angle of attack
$\alpha_1 ... \alpha_5$ = Runge-Kutta control parameters

Paper accepted July, 2004. Technical Editor: Aristeu Silveira Neto.

Δt = Time step value
λ = Characteristic speed
μ = Dynamic viscosity coefficient
ρ = Dimensionless density
ξ, η, ζ = General curvilinear coordinates

Subscripts

∞ = Freestream property
i, j, k = Grid node coordinates

Superscripts

ℓ = Runge-Kutta stage counter

Theoretical Formulation

The numerical code used solves the thin-layer approximation of the 3-D, compressible, laminar Navier-Stokes equations. These equations can be written in strong conservation-law form for general, body-conforming, curvilinear coordinates (Pulliam and Steger, 1980), as

$$\frac{\partial \overline{Q}}{\partial t}+\frac{\partial\left(\overline{E}-\overline{E}_v\right)}{\partial \xi}+\frac{\partial\left(\overline{F}-\overline{F}_v\right)}{\partial \eta}+\frac{\partial\left(\overline{G}-\overline{G}_v\right)}{\partial \zeta}=0\,, \tag{1}$$

where the vector of conserved quantities, $\overline{Q}$, is defined as

$$\overline{Q}=J^{-1}\left[\rho \quad \rho \mathrm{u} \quad \rho \mathrm{v} \quad \rho \mathrm{w} \quad \mathrm{e}\right]^T. \tag{2}$$

The formulation for the inviscid flux vectors, $\overline{E}$, $\overline{F}$ and $\overline{G}$, and the viscous flux vectors, $\overline{E}_v$, $\overline{F}_v$ and $\overline{G}_v$ can be found in Bigarelli, Mello and Azevedo (1999).

In the case of the viscous flux vectors, despite the inclusion of the viscous terms in the ξ and ζ directions, all cross derivative terms were not considered in this formulation. Moreover, the meshes used in the simulations do not give support to viscous dissipation in those directions. Therefore, the formulation should be referred to as a thin-layer model. Throughout this work, the curvilinear coordinate system is defined such that ξ is the rocket longitudinal direction, positive downstream, η is the wall-normal direction, and ζ is the circumferential direction. Expressions for the Jacobian of the transformation, J, and for the various metric terms can be found in Pulliam and Steger (1980), among other references. The Reynolds number, based on the freestream speed of sound, a_∞, density, ρ_∞, viscosity, μ_∞, and vehicle diameter, d, is given as $\mathrm{Re} = \rho_\infty a_\infty d/\mu_\infty$. More details of the present formulation can be found in Bigarelli, Mello and Azevedo (1999).

Numerical Implementation

The governing equations are discretized in a finite difference context. The spatial discretization adopted uses a central difference algorithm plus explicitly added artificial dissipation terms in order to control nonlinear instabilities. The equations, fully discretized in space, can be written as

$$\left(\frac{\partial \overline{Q}}{\partial t}\right)_{i,j,k}=-RHS_{i,j,k}\,. \tag{3}$$

The right-hand side operator of Eq (3) is defined as

$$\begin{aligned}
RHS_{i,j,k} = & \\
= & \frac{\overline{E}_{i+1,j,k}-\overline{E}_{i-1,j,k}}{2\Delta\xi}-\frac{E_{v_{i+\frac{1}{2},j,k}}-E_{v_{i-\frac{1}{2},j,k}}}{\Delta\xi} \\
& +\frac{\overline{F}_{i,j+1,k}-\overline{F}_{i,j-1,k}}{2\Delta\eta}-\frac{\overline{F}_{v_{i,j+\frac{1}{2},k}}-\overline{F}_{v_{i,j-\frac{1}{2},k}}}{\Delta\eta} \\
& +\frac{\overline{G}_{i,j,k+1}-\overline{G}_{i,j,k-1}}{2\Delta\zeta}-\frac{\overline{G}_{v_{i,j,k+\frac{1}{2}}}-\overline{G}_{v_{i,j,k-\frac{1}{2}}}}{\Delta\zeta} \\
& -\frac{J^{-1}_{i+\frac{1}{2},j,k}\,d_{i+\frac{1}{2},j,k}-J^{-1}_{i-\frac{1}{2},j,k}\,d_{i-\frac{1}{2},j,k}}{\Delta\xi} \\
& -\frac{J^{-1}_{i,j+\frac{1}{2},k}\,d_{i,j+\frac{1}{2},k}-J^{-1}_{i,j-\frac{1}{2},k}\,d_{i,j-\frac{1}{2},k}}{\Delta\eta} \\
& -\frac{J^{-1}_{i,j,k+\frac{1}{2}}\,d_{i,j,k+\frac{1}{2}}-J^{-1}_{i,j,k-\frac{1}{2}}\,d_{i,j,k-\frac{1}{2}}}{\Delta\zeta},
\end{aligned} \tag{4}$$

where $\Delta\xi=\Delta\eta=\Delta\zeta=1$ for the general curvilinear coordinate case. An anisotropic scalar artificial dissipation method (Turkel and Vatsa, 1994) was used. This scheme is nonlinear and allows a selection between artificial dissipation terms of second and fourth differences, which is very important in capturing shock waves in the flow. In Eq.(4), the artificial dissipation is represented by the d terms.

Time march uses an explicit, second-order accurate, five-stage Runge-Kutta scheme (Jameson, Schmidt and Turkel, 1981; Jameson and Mavriplis, 1986), which can be written as

$$\begin{aligned}
\overline{Q}^{(0)}_{i,j,k} &= \overline{Q}^{n}_{i,j,k} \\
\overline{Q}^{(\ell)}_{i,j,k} &= \overline{Q}^{(0)}_{i,j,k}-\alpha_\ell \Delta t_{i,j,k} RHS^{(\ell-1)}_{i,j,k} \\
\overline{Q}^{n+1}_{i,j,k} &= \overline{Q}^{(5)}_{i,j,k}
\end{aligned} \tag{5}$$

where $\ell = 1,2,...,5$. Numerical values for the parameters can be found in Jameson and Mavriplis (1986). In the previous expressions, Δt stands for the time step, and n and $n + 1$ refer to the property values at the start and at the end of each time step, respectively.

Equation (5) also indicates that a local time step option is being used in order to accelerate convergence to steady state calculations. This implementation is performed by means of the *CFL* definition for a general coordinate system. The time step can be given in terms of the *CFL* number, as

$$\Delta t_{i,j,k}=\frac{CFL}{\lambda}, \tag{6}$$

where the *CFL* number should be provided by the user and λ is a local characteristic speed, defined by the eigenvalues of the set of equations. More details of this implementation can be found in Bigarella (2002).

Boundary Conditions and Computational Grids

For the configurations of interest here, the types of boundary conditions that should be considered include solid wall, farfield, symmetry, upstream centerline and downstream (exit) conditions. For the rocket wall, the velocity vector is set to zero, and a zero-th order extrapolation of the pressure and the density is performed. The upstream centerline is a singularity of the coordinate transformation and, hence, an adequate treatment of this boundary must be provided. In the present case, the approach consists in extrapolating the property values from the adjacent longitudinal plane and in averaging the extrapolated values in the azimuthal direction in order to define the updated properties at the upstream centerline. At the exit plane, the boundary conditions are implemented through the use of the 1-D characteristic relations for the 3-D Euler equations. The interested reader is referred to Azevedo, Fico and Ortega (1995) for further details on the use of 1-D characteristic relations for boundary condition implementation. Freestream properties are assumed at the farfield boundaries.

Furthermore, in order to reduce computational costs, the grids used in the numerical simulations performed are generated for half a body in the azimuthal direction. This simplification is valid for the cases assessed in this work because low angles of attack are considered. This condition implies a symmetric flow about the pitching plane, as indicated in Ying (1986) among other references. Hence, symmetry is applied in the pitching plane using two auxiliary planes, namely, k = 1 and k = kmax. Those extra planes are added, respectively, before the leeside and after the windside pitching plane.

The final grid for the VLS main body configuration to which numerical results are mesh independent had 156 x 65 x 21 points. It must be emphasized that extensive mesh influence studies have been performed for flow simulation over the VLS configuration in the past, and the interested reader is referred to Azevedo and Buonomo (1999) and Basso, Antunes and Azevedo (2000a) for a more detailed account of some of these mesh refinement studies, for axisymmetric and 3-D flows, respectively. In the present work, these mesh influence studies have been extended and, as stated, the mesh for which results are discussed here is the one that yielded grid independent aerodynamic coefficients. The computational mesh for the Sonda III-A configuration had the same number of points. A view of a longitudinal plane of these grids is shown in Fig. 1. As in the VLS case, mesh refinement studies have been performed and the selected grid yields solutions which are mesh independent. The computational grids for the VLS and the Sonda III-A cases are very similar to each other, and they have been constructed to have about 20 points inside the boundary layer, with an exponential growth ratio of 20% along the normal direction to the wall.

Pressure Coefficient Results

In this section, the numerical simulations of the flow over the VLS second stage flight configuration at freestream Mach numbers M_∞ = 1.25 and 3.00, and angles of attack α = 0 and 4 deg. are presented. The computations are compared to available experimental data, obtained through wind tunnel tests. This comparison is necessary to assess the correctness of the numerical method developed such that it can be used to obtain aerodynamic data for vehicles to which no experimental data are available. In general, good agreement between the numerical and the experimental results is obtained, and numerical curves are qualitatively similar to the experimental ones.

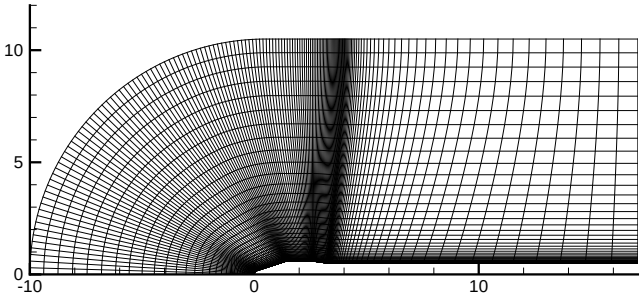

(a) VLS

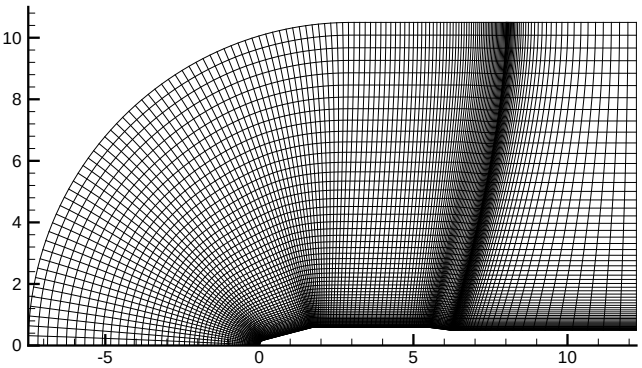

(b) Sonda III-A

Figure 1. Overall view of a plane from 3-D grids used.

A comparison between the computational results and available experimental data can be seen in Fig. 2. Pressure coefficient, C_p, distributions for two different longitudinal rocket planes, which are the vehicle leeward and windward generators, are presented. This figure shows the results for the flow over the VLS central body at freestream conditions α = 0 deg., Re = 30 million, and M_∞ = 1.25. These results indicate that the experimental data and the computational solution do not present large differences. In particular, the correct trends in the *Cp* distribution are captured by the numerical simulation. One can observe that the most relevant discrepancy between computation and experiment, which can be seen in Fig. 2, occurs at the end of the boattail, *i.e.*, at the boattail-afterbody cylinder intersection. However, one must also observe that, in this region of the flow, there is an oblique shock wave that impinges upon the body boundary layer. The fully correct account for this interaction would require an adequate turbulence model. Nevertheless, even in such regions, the discrepancies are quite small, as one can see in Fig. 2. Several other similar comparisons, at different flight conditions, are available for flow simulations over the VLS. However, the comparison shown in Fig. 2 is representative of the level of agreement which can be obtained between the experimental data and the computational simulation results throughout the speed range analyzed.

Similar *Cp* results for the VLS configuration at a higher freestream Mach number, namely M_∞ = 3.00, are shown in Fig. 3. This is a more demanding test case for the solver since, at this flight condition, strong shock waves are present in the flow. As in the previous case, the angle of attack is zero and the Reynolds number is Re = 30 million.

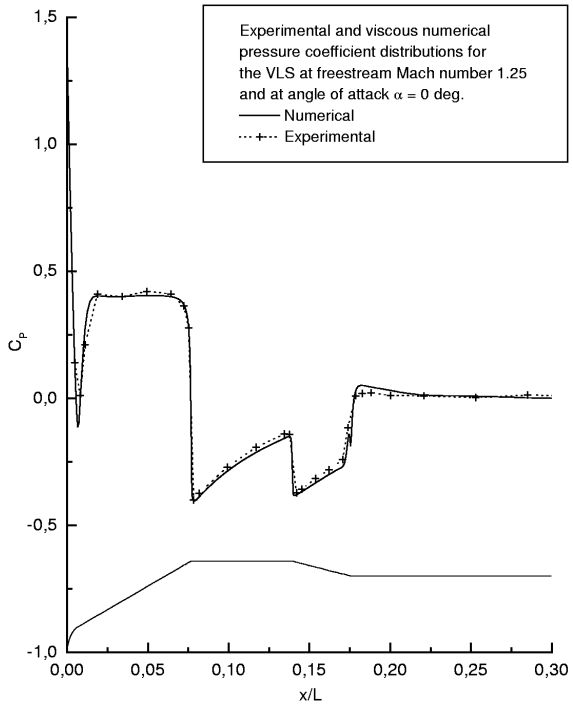

Figure 2. Numerical *Cp* distributions compared to experimental data for the VLS central body at α = 0 deg. and M_∞ = 1.25. Reynolds number is 30 million.

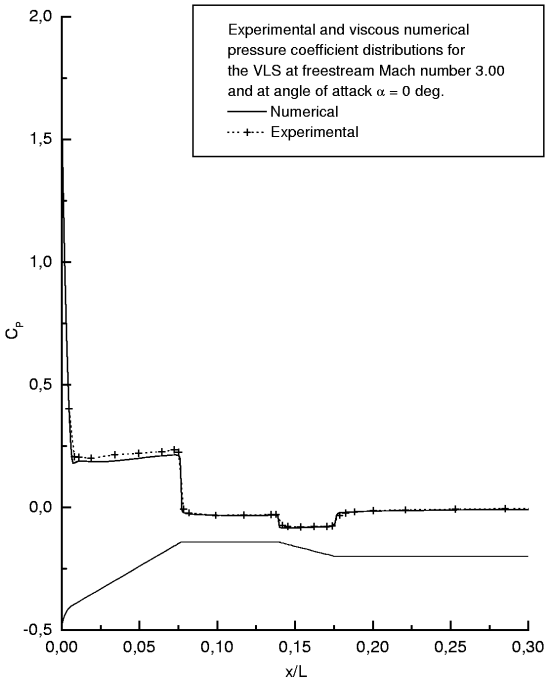

Figure 3. Numerical *Cp* distributions compared to experimental data for the VLS central body at α = 0 deg. and M_∞ = 3.00. Reynolds number is 30 million.

Figure 4 shows *Cp* distributions over the VLS second stage flight configuration at an angle of attack α = 4 deg., *Re* = 30 million, and freestream Mach number M_∞ = 1.25. Here, results are presented for the vehicle lee- and windside. In this case, since a positive angle of attack is considered, one can observe that the windside pressures are higher than the leeside ones, as expected. In general, one can observe in Fig. 4 that the agreement between numerical and experimental data is fairly good throughout the vehicle, except around the boattail-afterbody cylinder intersection. As previously discussed, an interaction between shock wave and boundary layer exists in this region and this is of fundamental importance for the local flow configuration. However, the levels of approximation of the formulation used in the numerical code presented here are not yet detailed enough to represent this interaction correctly. Similar distributions for the VLS central body at a higher freestream Mach number, namely M_∞ = 3.00, are presented in Fig. 5. As in the previous case, the angle of attack is α = 4 deg. and the *Cp* distributions are presented for the vehicle lee- and windside planes.

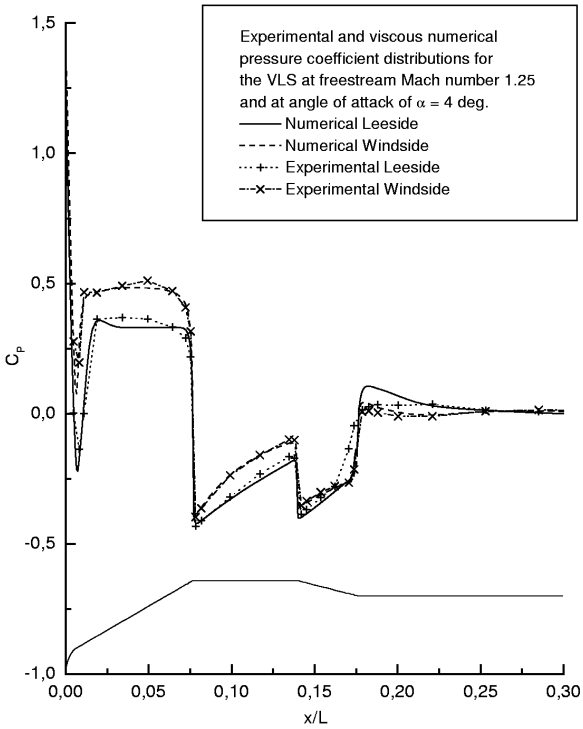

Figure 4. Numerical *Cp* distributions compared to experimental data for the VLS central body at α = 4 deg. and M_∞ = 1.25. Reynolds number is 30 million.

Normal Force Coefficient Results

For actual applications in design, one is typically concerned with the running normal loads and not with the local pressure distributions. Hence, circumferential integrations of the pressure coefficient distributions were performed to obtain the running normal force coefficients. These normal forces are calculated for different angles of attack such that the normal force coefficient slope can also be obtained. Further details on the procedure adopted for calculation of the normal force coefficients can be seen in Bigarelli, Mello and Azevedo (1999). One should observe that several other vehicles are currently being developed, or improved, within the range of responsibilities of IAE. Due to budgetary constraint in the country, it is not always possible to take these other vehicles to the wind tunnel, especially because this typically means performing tests overseas. The approach which is currently being pursued is to use the experimental data available for the VLS to acquire confidence in the computational tools currently under

development. Hence, this flow simulation capability can be applied to the other vehicles of interest, since the overall configurations are not that different from the VLS central body. One of such derivative vehicles is the Sonda III-A (Bigarelli, Mello and Azevedo, 1999), which is a modified version of an existing sounding rocket. The normal force results obtained for the Sonda III-A under the present effort are being used for actual design work without experimental verification.

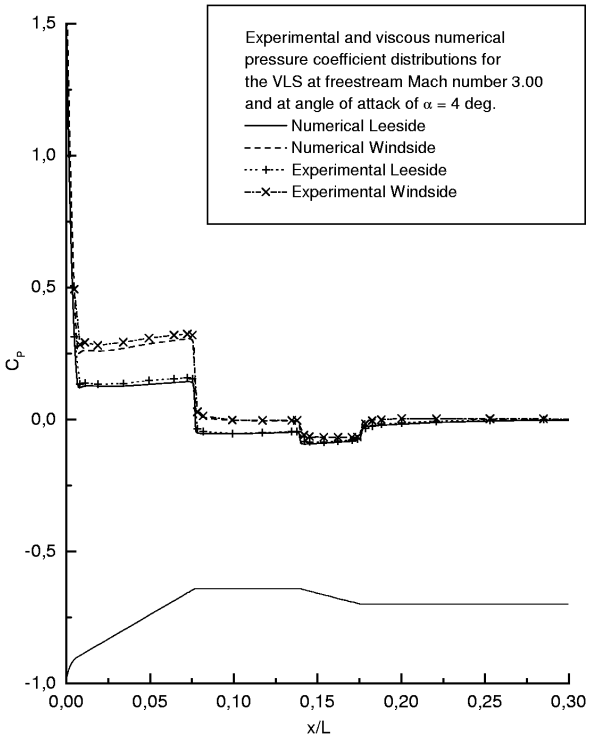

Figure 5. Numerical Cp distribuitions compared to experimental data for the VLS central body at α = 4 deg. and M_∞ = 3.00. Reynolds number is 30 million.

VLS Results

In this section, the running normal force coefficient distributions for the flow over the VLS second stage flight condition at freestream Mach numbers M_∞ = 0.90, 1.25, 2.00 and 3.00, and angles of attack α = 2 and 4 deg. are presented. For all supersonic cases, the freestream Reynolds number is *Re* = 30 million whereas, for the transonic case, it is *Re* = 25 million. The normal force distribution, dC_N/dx for the VLS central body at a freestream Mach number M_∞ = 1.25 is seen in Fig. 6. This figure presents the computational results compared to the experimental data for two different angles of attack, namely α = 2 and 4 deg. Numerical and experimental curves are qualitatively alike, except for the boattail region. As previously mentioned, aerodynamics in this region is very dependent on turbulent flow phenomena, such as boundary layer separation due to adverse pressure gradient and interactions between shock wave and boundary layer. Hence, it is expected that the level of approximation of the governing equations used in this work is not able to correctly simulate the exact flow behavior. Figure 7 shows similar results for the VLS at higher freestream Mach numbers. Flight conditions considered were freestream Mach number M_∞ = 2.00 and angles of attack α = 2 and 4 deg. One can verify that experimental and numerical curves are qualitatively similar to each other. However, in this case, it is possible to observe that there is a larger difference between computational and experimental data. This difference in the normal force coefficient distribution can be as large as 25% at some longitudinal stations along the VLS central body. Since these differences are considerably larger in this case, additional numerical studies have already been carried out in other recent efforts. It has been concluded, as presented in Bigarella (2002), that these differences are due to experimental result uncertainties, which are considerably large in this flow case, as discussed in that work.

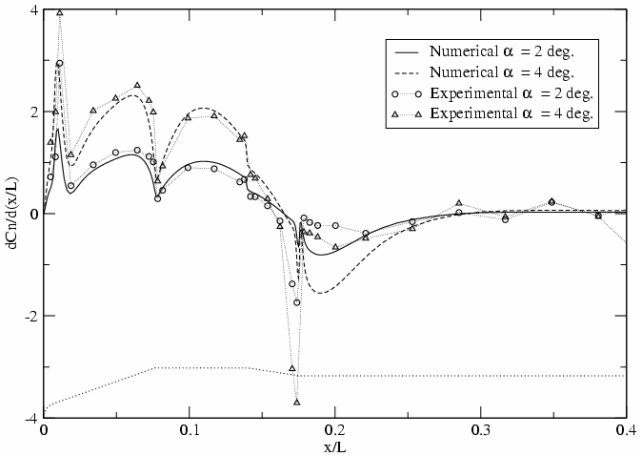

Figure 6. Running normal force coefficients obtained with the viscous formulation compared to experimental data for the VLS central body at M_∞ = 1.25, *Re* = 30 million and at two different angles of attack.

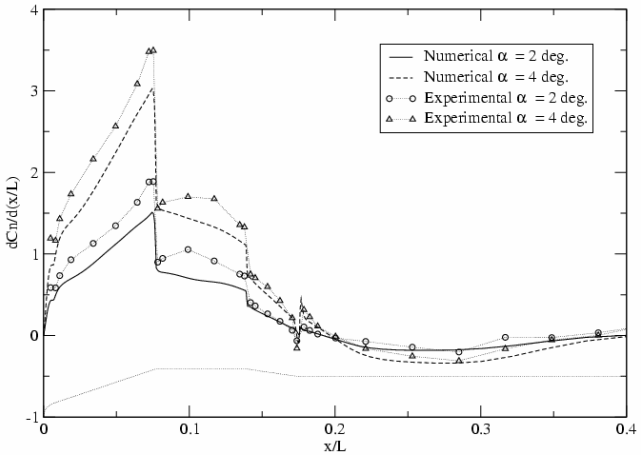

Figure 7. Running normal force coefficients obtained with the viscous formulation compared to experimental data for the VLS central body at M_∞ = 2.00, *Re* = 30 million and at two different angles of attack.

Running normal loads were also calculated for the vehicle at freestream Mach number M_∞ = 3.00 and at the same angles of attack as in the previous cases. One can see a comparison between numerical and experimental results in Fig. 8. This case has stronger shock waves present in the flow and, hence, it is a more challenging test case for the numerical code. One can observe, however, that the trends of the running normal load coefficient distributions are well captured by the code.

Another highly demanding test case is a transonic flight condition. Running normal force loads were obtained for the VLS at freestream Mach number M_∞ = 0.90 and angles of attack α = 2 and 4 deg. Numerical and experimental results for this simulation are presented in Fig. 9. In this case, a strong shock wave builds up over the payload fairing region and it is not attached to any geometric

discontinuity. Large differences between computational and experimental data can be observed in Fig. 9. This is another example of the influence of the boundary layer-shock wave interaction in the flow configuration. Preliminary turbulent results, in terms of pressure coefficient distributions, are already available for this flow condition and show much better agreement with experimental data (Bigarelli and Azevedo, 2002).

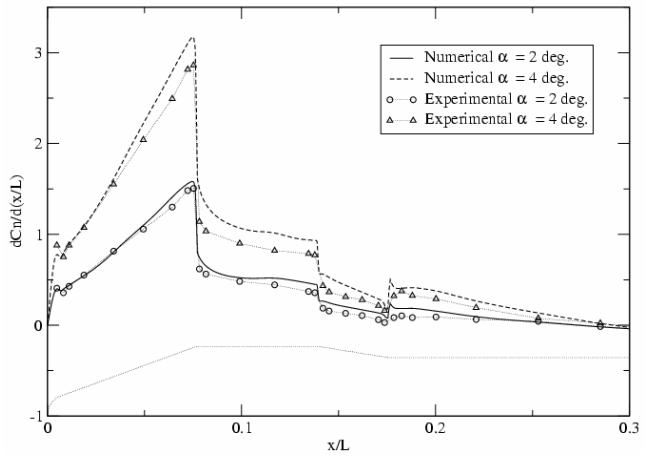

Figure 8. Running normal force coefficients obtained with the viscous formulation compared to experimental data for the VLS central body at M_∞ = 3.00, *Re* = 30 million, and at two different angles of attack.

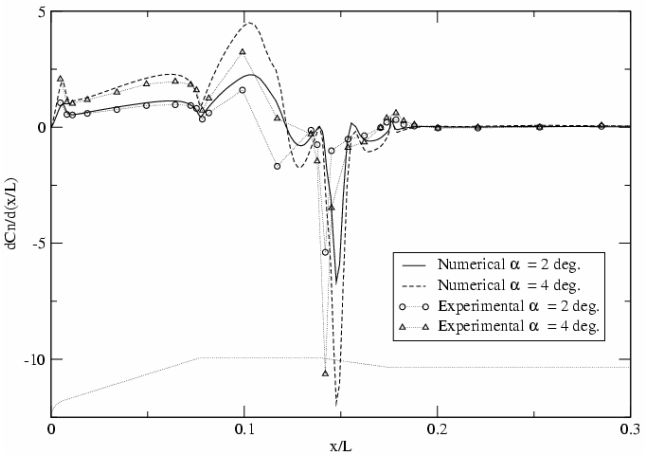

Figure 9. Running normal force coefficients obtained with the viscous formulation compared to experimental data for the VLS central body at M_∞ = 0.90, *Re* = 25 million, and at two different angles of attack.

The running normal force coefficient slope is obtained as the slope of dC_N/dx vs. α at a given crossflow plane. Since this work deals with small angles of attack, the slope for a given section is approximated by the slope of the best linear-fit curve throughout the set of three points, one point for each angle of attack. Figure 10 presents numerical and experimental results concerning the running normal force coefficient slopes over the VLS central body. Freestream Mach numbers considered were M_∞ = 1.25, 2.00 and 3.00. It can be observed in this figure that both numerical and experimental curves are qualitatively alike. This behavior is to be expected since these normal force slopes are derived from the same normal force coefficients already presented here for the VLS configuration. Furthermore, the good agreement observed for M_∞ = 2.00 is a good indication that the numerical code is capturing the correct trends in the vehicle normal load slopes, even though the agreement of the actual running loads for this Mach number was not good, as indicated in Fig. 7.

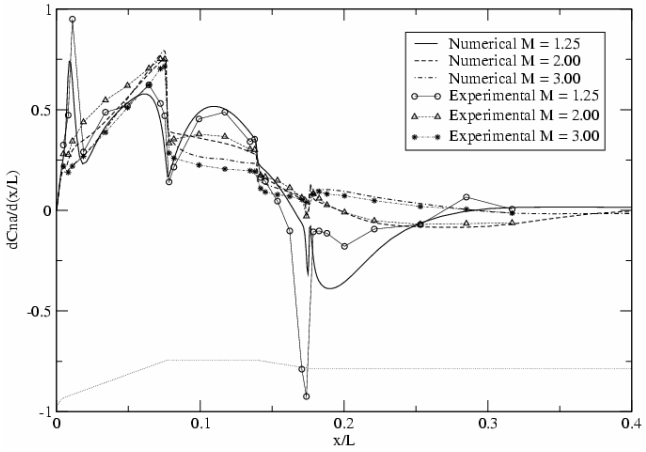

Figure 10. Numerical and experimental normal force coefficient slopes for the VLS at freestream Mach numbers M_∞ = 1.25, 2.00 and 3.00.

Table 1. Numerical and experimental integrated normal force coefficients, C_N, and normal force coefficient slopes, $C_{N\alpha}$, for the VLS central body.

M_∞	C_N				$C_{N\alpha}$ (1/deg.)	
	α = 2 deg.		α = 4 deg.			
	Num.	Exp.	Num.	Exp.	Num	Exp
1.25	0.0880	0.0937	0.1782	0.1928	0.0430	0.0467
2.0	0.1075	0.1424	0.2216	0.2652	0.0554	0.0607
3.0	0.1189	0.1321	0.2473	0.2793	0.0618	0.0710

The running normal force coefficient distributions can be integrated along the vehicle wall, resulting in the integrated normal force coefficient. This information is important to the design process as well as the running normal force distributions. Table 1 presents numerical and experimental integrated normal force coefficients. Obviously, a zero angle-of-attack condition yields zero normal force coefficients due to the flow symmetry. It can be observed that numerical values are smaller than the experimental ones. One can verify that the differences are usually of the order of 10% for the majority of the cases analysed. Nevertheless, as already discussed, the results for freestream Mach number M_∞ = 2.00 have a poorer correlation. Discrepancies for this Mach number are of the order of 25% for the α = 2 deg. case and 17% for the α = 4 deg. case. It should be observed that errors of about 10% can certainly be considered within the limitations of the level of approximation of the formulation here adopted.

Sonda III-A Results

In a very similar way as described for the VLS case, the running normal force coefficients over the Sonda III-A were also calculated. The running normal force coefficient distributions were integrated along the vehicle wall, resulting in the integrated normal force coefficient. Table 2 presents the numerical integrated normal force coefficients. As stated before, the zero angle-of-attack flight condition yields zero normal force coefficients, due to the flow symmetry.

Table 2. Integrated normal force coefficients, C_N, and normal force coefficient slopes, $C_{N\alpha}$, for the Sonda III-A.

M_∞	C_N		$C_{N\alpha}$
	α = 2 deg.	α = 4 deg.	
1.25	0.0886	0.1775	0.0444
2.00	0.0875	0.1856	0.0464
3.00	0.0906	0.1974	0.0494

It is important to emphasize that the work that led to the present paper has been originated from an actual need of obtaining aerodynamic data for the Sonda III-A configuration. Hence, the analysis of the VLS configuration was used to acquire confidence on the simulation capability available and to establish bounds on the errors, with regard to experimental data, that one would incur by the use of this level of formulation. Therefore, the Sonda III-A analysis was meant to generate actual engineering data that was used for the vehicle design, employing the simulation capability available in the CFD group at the time.

Concluding Remarks

This work presents the application of the capability implemented at IAE to solve 3-D flows over complex aerospace configurations at angle of attack to determine important aerodynamic loads required at the design stage. A computational code which solves the 3-D, thin-layer approximation of the compressible Navier-Stokes equations without turbulence closure for general, body-conforming, curvilinear coordinates is used. The numerical code is used to simulate flows about the VLS central body and the Sonda III-A configuration at freestream Mach numbers of 0.90, 1.25, 2.00 and 3.00, and angles of attack of 0, 2 and 4 deg.

Some initial analyses involved the comparison of computational results to available experimental data for the VLS main body configuration. In general, good agreement between the numerical and the experimental results was obtained. Nevertheless, in some regions of the flow, computational simulations were not able to capture the exact flow behavior. This can be explained by the fact that, in those regions, turbulence and interactions between shock waves and boundary layer are determinant for the flow configuration.

Some numerical results were presented for a configuration to which there are no available experimental data, since it is a new vehicle for which one cannot justify the extensive wind tunnel tests that would have to be performed overseas. Considering the good agreement, *i.e.*, within engineering error margins, obtained for the VLS case, the computational results for flows over the Sonda III-A could be used directly to the vehicle design stage.

Finally, as discussed in the paper, this work was originated from the real engineering need to provide estimates of the aerodynamic behavior of the Sonda III-A vehicle. Hence, the tools available at the time were used for this job, within the context here described. The authors are aware that a more complete analysis of these problems would require a turbulent formulation, due to the high flight Reynolds numbers of interest. Nevertheless, the results here included could be regarded as an account of the evolutionary process towards the complete flow simulation capability, as well as an example of the judicious use of a less than optimal formulation, for the problem at hand, in order to provide actual aerodynamic design data.

Acknowledgments

The present work was partially supported by Conselho Nacional de Desenvolvimento Científico e Tecnológico, CNPq, under the Integrated Project Research Grant No. 501200/2003-7. The authors are also indebted to Fundação de Amparo à Pesquisa do Estado de São Paulo, FAPESP, which provided a graduate scholarship to the first author.

References

Azevedo, J.L.F., and Buonomo, C.A., "Axisymmetric Turbulent Simulations of Launch Vehicle Forebody Flows", AIAA Paper No. 99-3528, 30th AIAA Fluid Dynamics Conference and Exhibit, Norfolk, VA, June-July 1999.

Azevedo, J.L.F., Fico, N.G.C.R., Jr., and Ortega, M.A., 1995, "Two-Dimensional and Axisymmetric Nozzle Flow Computations Using the Euler Equations", Journal of the Brazilian Society of Mechanical Sciences, Vol. 17, No. 2, pp. 147-170.

Azevedo, J.L.F., Moraes, P., Jr., Maliska, C.R., Marchi, C.H., and Silva, A.F.C., 1996, "Code Validation for High-Speed Flow Simulation over Satellite Launch Vehicle", Journal of Spacecraft and Rockets, Vol. 33, No. 1, pp. 15-21.

Azevedo, J.L.F., Zdravistch, F., and Silva, A.F.C., 1991, "Implementation and Validation of Euler Solvers for Launch Vehicle Flows", Proceedings of the Fourth International Symposium on Computational Fluid Dynamics, Vol I, Davis, CA, USA, pp. 42-47.

Basso, E., Antunes, A.P., Azevedo, J.L.F., 2000a, "Three Dimensional Flow Simulations Over a Complete Satellite Launcher with a Cluster Configuration",Proceedings of the 18th AIAA Applied Aerodynamics Conference and Exhibit, Denver, CO, USA, pp. 805-813.

Basso, E., Antunes, A.P., Azevedo, J.L.F., 2000b, "A Realistic Application of Computational Fluid Dynamics for the VLS Project", Proceedings of the 21st Iberian Latin American Congress on Computational Methods in Engineering - CILAMCE 2000, Rio de Janeiro, RJ, Brazil.

Bigarella, E.D.V., 2002, "Three-Dimensional Turbulent Flow Simulations over Aerospace Configurations", Master Thesis, Instituto Tecnológico de Aeronáutica, São José dos Campos, SP, Brazil.

Bigarelli, E.D.V., and Azevedo, J.L.F., 1999, "Calculation of the Aerodynamic Loads over the Sonda III-A Vehicle on Transonic and Supersonic Flow Conditions", Report No. 524-000000/B1001, Instituto de Aeronáutica e Espaço, São José dos Campos, SP, Brazil (in Portuguese).

Bigarelli, E.D.V., Mello, O.A.F., and Azevedo, J.L.F., 1999, "Three Dimensional Flow Simulations for Typical Launch Vehicles at Angle of Attack", Proceedings of the 15th Brazilian Congress of Mechanical Engineering - COBEM 99, Águas de Lindóia, SP, Brazil (publication in CD-ROM without page numbering).

Jameson, A., and Mavriplis, D., 1986, "Finite Volume Solution of the Two-Dimensional Euler Equations on a Regular Triangular Mesh", AIAA Journal, Vol. 24, No. 4, pp. 611-618.

Jameson, A., Schmidt, W., and Turkel, E., 1981, "Numerical Solution of the Euler Equations by Finite Volume Methods Using Runge-Kutta Time-Stepping Schemes", AIAA Paper 81-1259, AIAA 14th Fluid and Plasma Dynamics Conference, Palo Alto, CA, USA.

Pulliam, T.H., and Steger, J.L., 1980, "Implicit Finite-Difference Simulations of Three-Dimensional Compressible Flow", AIAA Journal, Vol. 18, No. 2, pp. 159-167.

Turkel, E., and Vatsa, V.N., 1994, "Effect of Artificial Viscosity on Three-Dimensional Flow Solutions", AIAA Journal, Vol. 32, No. 1, pp. 39-45.

Ying, S.X., 1986, "Three-Dimensional Implicit Approximately Factored Schemes for the Equations of Gasdynamics", SUDDAR 557, Department of Aeronautics and Astronautics, Stanford University, Stanford, CA, USA.

Zdravistch, F., and Azevedo, J.L.F., 1990, "Numerical Simulation of High Speed Flows over Complex Satellite Launchers", Proceedings of the 3rd Brazilian Congress of Engineering and Thermal Sciences (ENCIT), Itapema, Santa Catarina, Brazil, pp. 233-238.